Clays and Clay Minerals, Vol. 49, No. 6, 500–513, 2001.

THE Cs/K EXCHANGE IN MUSCOVITE INTERLAYERS: AN *AB INITIO* TREATMENT

KEVIN M. ROSSO*, JAMES R. RUSTAD AND ERIC J. BYLASKA

W.R. Wiley Environmental Molecular Science Laboratory,
Pacific Northwest National Laboratory, Richland, Washington 99352, USA

Abstract—Plane-wave pseudopotential total energy calculations have been applied to investigate the structure and energetics of the Cs/K exchange into interlayer sites in muscovite mica. Novel muscovite structures were designed to isolate the effects of 2:1 layer charge, cation size/interlayer site shape, and tetrahedral Al/Si substitutions on the exchange. All atom and cell-parameter optimizations were performed with the intention to mimic the constant pressure, non-isovolumetric exchange conditions thought to be found at frayed-edge sites. Under conditions where the cell parameters are allowed to relax, the overall Cs/K exchange reaction is surprisingly close to isoenergetic. The forward reaction is more strongly favored with increasing layer charge. For the condition of zero layer charge and no interlayer site distortion, the difference in the optimal interlayer spacing for Cs relative to K is very small, indicating a baseline indifference of the muscovite structure to cation size. The presence of 2:1 layer charge or tetrahedral rotations arising from Al/Si substitutions clearly change this outcome. Analysis of the dependence of the interlayer spacing on layer charge shows that while the spacing collapses with increasing layer charge for K as the interlayer cation, the reverse is true for Cs. We attribute the contrasting behavior to inherent differences in the ability of these cations to screen 2:1 layer-layer repulsions. Such effects might be involved during exchange at frayed-edge sites where interlayer spacings are increased. This is known, from experiment, to be very selective for Cs. Overall, the exchange energetics are so low that the Cs/K exchange rate and degree of irreversibility are likely to be dominated by diffusion kinetics.

Key Words:—*Ab Initio,* Cation Exchange, Cesium, Clay, Defects, Density Functional Theory, Exchange Energy, Isomorphic Substitution, Mica, Muscovite.

INTRODUCTION

The uptake of ^{137}Cs by naturally occurring layered silicate minerals is often the principal attenuation mechanism in the transport of this contaminant in subsurface environments. In natural waters, Cs is highly soluble and has no known solubility-limiting precipitates to limit its concentration in solution. It forms no strong surface complexes with silica (Kinniburgh and Jackson, 1981) or common Fe, Mn or Al oxides (Brueeuwsma and Lyklema, 1971; Venkataramani *et al.,* 1978; Anderson and Allard, 1983; Kim *et al.,* 1996). Cesium sorption to many mineral surfaces usually derives from the need for counterions to balance surface charge and is non-specific. Therefore, surface concentrations are easily modified by changes in solution conditions. However, Cs is found to be strongly associated and resistant to removal from certain sites on phyllosilicate minerals. While Cs only interacts weakly with basal surface and edge terminations of sheet silicate layers, partially delaminated zones adjacent to the edge termination of silicate sheets, so-called frayed-edge sites (Jackson, 1963; Rich and Black, 1964), provide sterically selective interlayer environments where Cs is held tightly with a high preference over many common compatible interlayer species (*e.g.* Cremers *et al.,* 1988; Comans *et al.,* 1991; De Preter *et al.,* 1991; Comans and Hockley, 1992; Gutierrez and Fuentes, 1996; Maes *et al.,* 1999; Bradbury and Baeyens, 2000). The exchange of Cs from solution for interlayer cations is facilitated by interlayer expansion and direct access of solution to these sites. Subsequent collapse of the interlayer spacing occupied by Cs effectively fixes this otherwise highly mobile species.

Cation exchange in the interlayer site of micas has been an intensely studied topic at the macroscopic scale. Pioneering work in the late 1950s and throughout the 1960s demonstrated the important influence of isomorphic substitutions and variability in layer charge (LC) on the cation exchange capacity (CEC), selectivity, interlayer expansion, and kinetics (*e.g.* Mortland, 1958; White *et al.,* 1962; Burns and White, 1963; Tamura *et al.,* 1963; Scott and Reed, 1964; Dolcater, 1968). A large body of experimental work exists on the uptake of Cs, in particular by phyllosilicate minerals, but comparatively little information is available regarding the local structure of Cs incorporated into interlayer environments and the various possible influences on the exchange reactions. Nuclear magnetic resonance (NMR) approaches have been fruitful in the identification of bonding environments for Cs in clay minerals (*e.g.* Weiss *et al.,* 1990; Kim *et al.,* 1996; Kim and Kirkpatrick, 1997). However, the effects of nearby isomorphic substitutions and variations in LC are difficult to isolate from such experiments. Molecular modeling techniques can be a useful means of gathering information in this regard, and can form a basis on which to interpret experimental data.

In this study, plane-wave pseudopotential density functional theory (DFT) calculations are used to investigate the energetics and structural modifications accompanying the exchange of Cs for K in the interlayer of muscovite mica. We focus on the initial and final states of exchange in this study and not the abundance of intermediate reactions that must occur because molecular dynamics simulation of exchange at the *ab initio* level of theory is currently not feasible. Empirical potential molecular dynamics or Monte Carlo simulations of aspects of cation exchange and interlayer water structure have only recently become available (*e.g.* Skipper *et al.,* 1991; Chang *et al.,* 1995; Bridgeman and Skipper, 1997; Greathouse and Sposito, 1998; Smith, 1998; Young and Smith, 2000; de Carvalho and Skipper, 2001; Wang *et al.,* 2001). The DFT total energy calculations have been applied successfully to phyllosilicates elsewhere (*e.g.* Bridgeman *et al.,* 1996; Hobbs *et al.,* 1997; Chatterjee *et al.,* 2000). Muscovite was chosen, partly because it is ubiquitous in sediments, it has a relatively simple structure in the interlayer region, and it has a high cation exchange selectivity for Cs. The DFT methods are applied to deal accurately with subtle variations in charge distribution, spatially separated charges, and to treat the variability in bond types (ranging from fully covalent to ionic) on equal footings. Structural optimizations of a variety of muscovite models were performed allowing all atom positions and unit-cell parameters to vary, without symmetry constraints. Lifting the constraints on the unit-cell parameters better mimics the freedom in the interlayer spacing expected at frayed-edge sites. Relative total energies for optimized structures are used to estimate the energetics for the overall exchange reaction for constant pressure (1 bar), non-isovolumetric conditions. In this regard, independent effects of LC, Al/Si tetrahedral substitutions and interlayer site structure are estimated.

THEORETICAL METHODS

Structures and total energies were calculated using the *ab initio* plane-wave pseudopotential method as implemented in CASTEP. The interested reader is referred to the review article by Payne *et al.* (1992) for a comprehensive introduction to this specific quantum mechanical modeling approach. Generalized gradient approximation (GGA) DFT was applied using the Perdew and Wang (1992) parameterization of the exchange-correlation functional, modified to work with plane-wave calculations (*e.g.* White and Bird, 1994). We used the CASTEP parameterization of ultrasoft pseudopotentials (Vanderbilt, 1990) without core corrections. Pseudopotentials were generated using the local density approximation (LDA) which means that the screening effect of the core electrons was modeled using LDA whereas the screening effect of the valence electrons was modeled using GGA. This approach has been validated previously (Garcia *et al.,* 1992). The atomic coordinates and cell parameters of model muscovite structures were optimized simultaneously completely free of symmetry restrictions (*i.e.* in the *P*1 space group). Optimized *c* axis dimensions were tested to be true energy minima by subsequent optimizations with slightly increased fixed *c* axis dimensions (*i.e.* under a tensile stress along *c*) and comparing calculated total energies. Two k points were used [0.25, 0.25, 0] and [0.25, −0.25, 0] which turned out to give similar energies to gamma point [0, 0, 0] calculations and were hence deemed converged with respect to k points. Gamma point calculations proved to give satisfactory results for closely related mineral structures (*e.g.* Bridgeman *et al.,* 1996; Chatterjee *et al.,* 2000). A pre-optimization strategy was followed by a more robust final optimization strategy. Pre-optimization was performed using a lower cut-off energy (300 eV) and a conjugate gradient electronic minimizer using a density mixing scheme (Kresse and Furthmuller, 1996). Final optimizations were run using 380 eV and an all-bands electronic minimizer (Gillan, 1989). This approach was designed to overcome potential problems with achieving convergence associated with the discontinuously changing number of plane waves as the cell parameters vary. The relative total energy differences found for the exchange reactions varied little from the pre-optimized to the final optimization runs. Finite basis set error estimations using methods described in Payne *et al.* (1992) were < 0.1 eV/atom, indicating that the calculations are converged with respect to basis set size and should produce usefully accurate total energies (Cerius^2 User Guide, 1997). Single-point total energy calculations on the gas-phase atoms were run using the final optimization strategy as described above except with the density mixing minimizer. Total energies for the gas-phase atoms are converged with respect to unit-cell size (*i.e.* box size effects are insignificant).

DESCRIPTION OF THE EXCHANGE SYSTEM

The muscovite structure

The structure of muscovite can be described as stacks of so-called 2:1 layers (Figure 1) which consist of two sheets of corner-sharing SiO_4 tetrahedra that sandwich one sheet of edge-sharing AlO_6 octahedra, giving T-O-T layers. The tetrahedral sheets are linked siloxane rings that have six-fold symmetry if undistorted. Apical oxygens point towards the octahedral sheet and constitute all but one of the necessary oxygen atoms to form the octahedral cavities, which are completed by a hydroxyl group located laterally at centers of siloxane rings. Aluminum occupies two of the three available octahedral cavities, with the remaining one vacant, leading to the dioctahedral classification. The structure is complicated by the fact that

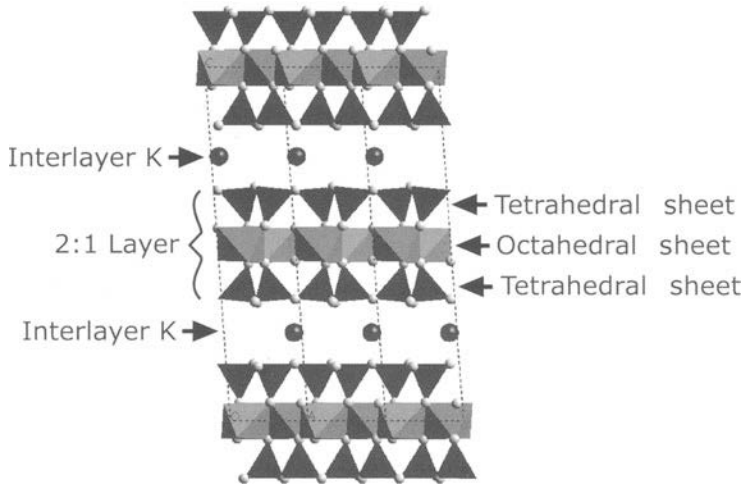

Figure 1. A polyhedral structure model depicting the structure of muscovite. Tetrahedral sheets are composed of corner-sharing silicate tetrahedra, which sandwich edge-sharing Al octahedra. The 2:1 layers are stacked and keyed together at siloxane cavities, where interlayer K resides. Layer charge derives from Al/Si substitutions in tetrahedral sheets.

the 2:1 layers are charge neutral units ($Al_2Si_4O_{10}(OH)_2$ as in pyrophyllite), unless Si atoms are partially replaced by Al atoms in the tetrahedral sites. Each Al → Si substitution effectively creates a permanent free electrical charge at the surface of the 2:1 layer, which is compensated by the presence of a monovalent interlayer cation, K in the case of muscovite. The distribution of Al/Si substitution is typically not long-range ordered. Short-range ordering (several unit-cells) is possible (Bailey, 1984), and is probably influenced by Loewenstein's rule (*i.e.* the avoidance of Al_{tet}–O–Al_{tet} linkages). Because the LC that binds the interlayer cation is dependent on the Al/Si substitution, it is reasonable to assume that the exchange reaction is influenced by proximity of the exchange site to AlO_4 tetrahedra. In the open literature, such relationships are often presumed, but direct supporting evidence is rare because of the difficulty in obtaining it. In this study, we attempt to elucidate any such effects by considering more than one explicit arrangement of Al/Si substitution locations in the unit-cell. Including Al/Si substitution, the formula unit then becomes $KAl_2(Al,Si_3)O_{10}(OH)_2$.

In building up the muscovite structure along the *c* axis, repeating 2:1 units are stacked and keyed together at the siloxane cavities. This creates 12-fold coordinated sites for interlayer cations consisting of six short and six long *M*–O bonds. Several stacking sequences of 2:1 units are possible, leading to polytypism in the micas (see Bailey, 1984). In muscovite, 2:1 layers are commonly stacked by alternating 2:1 layers rotated by either 0° or 120° with respect to each other, a characteristic of the $2M_1$ polytype, giving a monoclinic structure where $\alpha = \gamma = 90°$ ($\neq \beta$, $a \neq b \neq c$) and the space group *C*2/*c*. In the absence of other distortions, this arranges the six short *M*–O bonds in a regular octahedral fashion about the interlayer cation site. The Cs end-member analogue to muscovite is nanpingite and is a $2M_2$ polytype having stacking displacement vectors at 60° or 180° to each other (Ni and Hughes, 1996). This arranges the six short *M*–O bonds in a ditrigonal prism about the interlayer cation. The interlayer site structure in nanpingite is suggestive of a preferred bonding environment for Cs that cannot be obtained during localized interlayer exchange in the muscovite structure without significant distortion. In this study, calculations of Cs-substituted structures are based on exchange into the $2M_1$ polytype.

Representative model structures

The structure of muscovite is normally reported in terms of the conventional unit-cell parameters. The conventional unit-cell has two lattice points at (0 0 0) and (½, ½, 0) and four formula units ($Z = 4$). It is important to recognize that this choice of basis vectors does not lead to the smallest possible unit-cell. To reduce the computational expense we performed all our calculations on the primitive unit-cell which halves the number of atoms ($Z = 2$). The transformation that gives the primitive basis is $a_p = 0.5a_c - 0.5b_c + 0.0c_c$, $b_p = 0.5a_c + 0.5b_c + 0.0c_c$, $c_p = 0.0a_c + 0.0b_c + 1.0c_c$ where subscripts p and c refer to the primitive and conventional bases, respectively. Results of calculations will be principally discussed in terms of the primitive unit-cell (but note the equivalence of the *c* axes), and optimized structural data are reported in terms of the conventional unit-cell in an Appendix.

Four models of the muscovite structure based on the primitive unit-cell were constructed with expected different affinities for interlayer cations (Figure 2). In each model, only one of the two possible K interlayer sites was treated as the exchange site. The occupation

https://doi.org/10.1346/CCMN.2001.0490603 Published online by Cambridge University Press

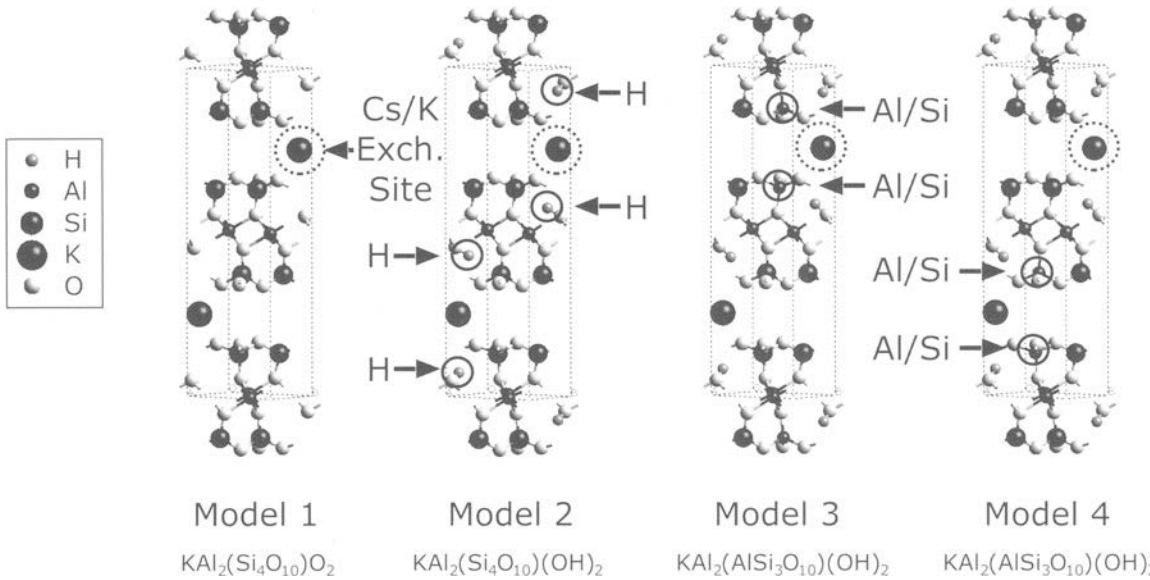

Figure 2. Ball and stick models for the four types of muscovite structures used in this study. Models 1 and 2 are not formally charge-balanced structures by design and differ by the incorporation of H in the latter. Models 1 and 2 have effective −2 and 0 LCs, respectively. Models 3 and 4 both have H and Al/Si substitutions giving LCs of −1 but differ in Al/Si substitution locations. The interlayer cation exchange site for the calculations in this study is denoted by a dashed circle. The lower interlayer site is occupied by K for all the calculations.

of the other was fixed as K throughout so that the effects of a single replacement could be isolated. Hence, calculated expansions of the structure along the *c* axis are presumably half of the expansion that would result from complete exchange of Cs into both interlayer sites in the unit-cell. Models 1 and 2 do not involve Al/Si substitution; model 3 has two Si atoms replaced by Al at opposing sides of the Cs/K exchange site across the basal plane; and model 4 has two similar replacements at the K interlayer site adjacent to the Cs/K exchange site. Because we restricted our calculations to the smallest possible unit-cell, each Al/Si substitution transforms the occupation of a tetrahedral sheet into $Si_{0.5}Al_{0.5}$.

Models 3 and 4 are formally charge balanced and match the stoichiometry of muscovite, but models 1 and 2 are not formally balanced. The formula units of models 1 and 2 have formal net charges of −1 and +1, respectively, with the difference due to the inclusion of hydrogen atoms in the latter (Figure 2). By necessity, for most periodic method *ab initio* calculations in practice, because the unit-cell is treated as infinitely repeating, the net charge on the unit-cell must be neutral so as to avoid a catastrophic divergence of Coulombic energy terms. Forcing this neutrality condition on models 1 and 2 means that model 1 is slightly electron depleted (by 1 $e-$ per formula unit) and model 2 has a slight electron excess (by 1 $e-$ per formula unit) relative to models 3 and 4 which saturate every 2:1 LC with an interlayer cation with formal charge balance. Models 1 and 2 then differ substantially in their electrostatic affinity for an interlayer cation, with 2:1 layers in model 1 having a high affinity (LC = −2) and that in model 2 (LC = 0) having a low affinity. And, because the charge balance deviations are not atom specific, these deviations are distributed homogeneously over 2:1 layer atoms, which presumably differs from the localized layer charging associated with tetrahedral Al/Si substitutions found in models 3 and 4 (LC = −1). By design then, the models allow one to probe the effects of variable electrostatic affinities and the degree of localization of LC on the interlayer site and cation exchange energetics. Although models 1 and 2 are not formally charge balanced, because of the predominance of disorder in isomorphic substitutions in micas, it seems possible that such stoichiometries could be present as subdomains within larger, charge-balanced supercells of muscovite.

The exchange model

The overall Cs/K exchange at interlayer sites can be decomposed into several general steps: (1) opening of the interlayer spacing (delamination); (2) hydration and release of interlayer K; (3) sorption and dehydration of Cs; and (4) closing of interlayer spacing. The process is facilitated naturally at frayed-edge sites where solution has easy access to interlayer spaces (Figure 3). Molecular-scale processes leading to the opening of the interlayer spacing at the muscovite edge-solution interface are currently poorly understood, but it is envisioned that such an opening must precede the exchange reaction to accommodate diffu-

https://doi.org/10.1346/CCMN.2001.0490603 Published online by Cambridge University Press

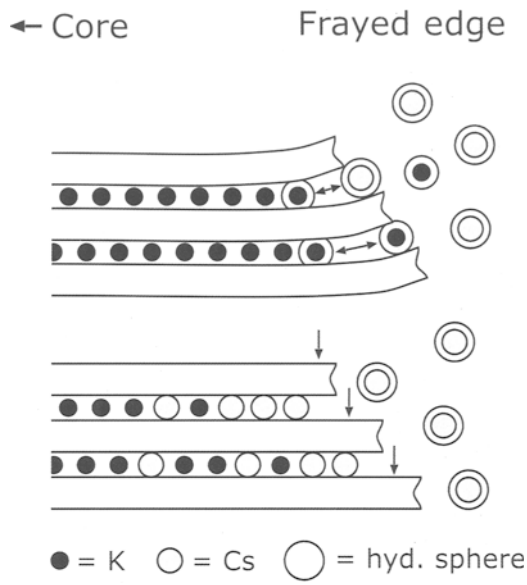

Figure 3. An illustration of the Cs/K exchange at frayed-edge sites. Cs-bearing aqueous solution gains access to interlayer sites at opened interlayer spacings near the termination of 2:1 layers. Hydration, desorption and outward diffusion of K is accompanied by inward diffusion, adsorption, and dehydration of Cs during exchange. Dehydration of Cs at frayed-edge sites collapses the interlayers, effectively fixing Cs.

sion of the exchanging cations. Relevant literature is available on molecular interlayer swelling mechanisms (*e.g.* Shroll and Smith, 1999; Smith, 1998; Young and Smith, 2000) and macroscopic treatments have been proposed (Laird, 1996, 1999), but this important step is not the focus of the current study. In this study, to address the overall energetics of the exchange reaction, we concern ourselves only with the initial and final states. The initial state consists of interlayer K in the muscovite structure and Cs in aqueous solution at infinite separation. The final state consists of interlayer Cs in muscovite and K in aqueous solution at infinite separation. This approach essentially reduces the contributions to the exchange reaction into the relative energy differences for K and Cs to be solvated by aqueous solution and to be incorporated into the muscovite structure.

The necessary calculations are shown schematically in Figure 4. Four total energy calculations are performed for each model type. Two are for the geometry-optimized solid phases before and after exchange and two are for K and Cs in the gas phase. Because of the charge-neutral unit-cell constraint, the total energies for the free monovalent cations were substituted with neutral atom total energies. The enthalpic (ΔH) and entropic (ΔS) energy corrections required to mod-

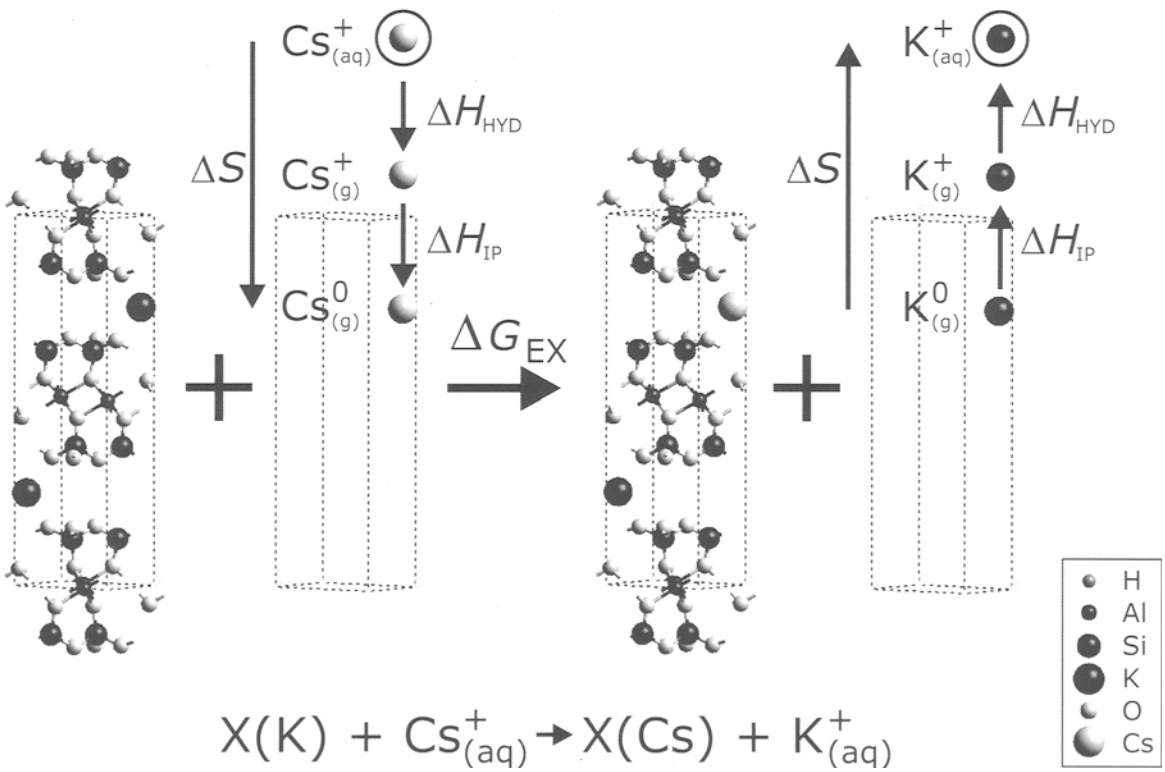

Figure 4. The steps and necessary calculations to estimate the overall Cs/K exchange energetics. Total energies for the muscovite structures and the gas-phase neutral K and Cs atoms are obtained from the *ab initio* calculations. The ΔH and ΔS values are obtained from tabulated experimental data (Wagman *et al.*, 1968, 1969).

https://doi.org/10.1346/CCMN.2001.0490603 Published online by Cambridge University Press

ify the free cation energetics for the monovalent solvated state are indicated in Figure 4. Explicit calculation of these corrections requires knowledge of the structure of the hydration sphere around each of the cations in water, a difficult modeling task because these are large, highly polarizable cations. In the hydration sphere, the strength of the metal-water interaction is comparable to the strength of water-water interactions (Feller *et al.,* 1995). This leads to many possible local minima for the conformation of the hydration sphere energetically near the global minimum, making an explicit calculation of the hydration energy expensive and of questionable practical usefulness for this study. Instead, we estimate the value of the energy corrections using tabulated experimental thermodynamic data (Wagman *et al.,* 1968, 1969), which are more than sufficiently accurate to be meaningful compared to the theoretical total energy differences.

It should be noted that, because of the periodic theoretical method and the restriction of having to use the minimum muscovite cell, the exchange energy that is calculated is that for replacing one full interlayer of cations. Possible energy contributions from stresses on 2:1 layers due to a mixed Cs/K occupation of a plane of interlayer sites are therefore neglected.

RESULTS AND DISCUSSION

Pre-exchanged muscovite

Structural parameters for the optimized pre-exchange muscovite models are listed in Table 1 (conventional cell parameters can be found in the Appendix). Although the optimizations were performed without symmetry constraints, the structures converge to the appropriate space groups to within a 0.05 Å search tolerance (models 1 and 2 = *C*2/*c,* models 3 and 4 = *C*2). The average Si–O bond length obtained varied insignificantly from 1.607 Å between the models, which compares reasonably well with the known mean tetrahedral Si–O bond length of 1.626 Å for most silicate minerals (Gibbs, 1982). Overall, the unit-cell parameters predicted for all the pre-exchanged muscovite models are in good agreement with data from structure refinements. The conventional cell axes *a* and *b* and α, β, γ agree with experiment to within 1%. The *c* axes agree to within 4%. These results suggest that the theoretical method applied performs satisfactorily for this system.

In an analysis of the set of structures, of particular interest was whether or not trends could be found between the cell parameters, interlayer site dimensions, and the built-in variability in LC. For models 1 and 2, where no tetrahedral substitutions are included, predictable structural changes were found occurring primarily along the direction normal to the basal plane, consistent with the softer direction in the structure. The basal dimensions, controlled primarily by the octahedral sheet (Bailey, 1984), are rigid by comparison and were found to vary little (Table 1). Model 1 leads to the most compact structure, having a unit-cell volume more than 15 $Å^3$ smaller and the *c* axis cell edge ~0.6 Å shorter than that for the other models. For model 2, an expanded structure results, having the largest unit-cell volume and a significantly longer *c* axis than model 1.

The interlayer separation does not lend itself to unambiguous measurement because of a characteristic out-of-plane rotation for tetrahedral groups arising from the natural lattice mismatch between the tetrahedral and octahedral sheets. This tetrahedral tilting corrugates the basal plane of 2:1 layers. Here we define the interlayer separation as the average of three of the prismatic O–O distances from the 12-fold polyhedron across an interlayer site (along the basal plane normal direction), where the O–O pairs are related spatially by ~3-fold rotation when viewed down the direction normal to the basal plane. Interlayer spacings are given in Table 2. The average of the two interlayer separations in model 1 is 3.64 Å, whereas it is 3.88 Å in model 2. Therefore, 80% of the contraction of the *c*-axis cell edge found in model 1 relative to model 2 is accounted for by a change in the interlayer spacings, with slight 2:1 layer thinning accounting for the rest.

For models 1 and 2, we attribute the differences in the interlayer spacing solely to the built-in differences in LC. There are two convenient ways to understand this effect. Based on the stoichiometry of model 1, 2:1 layers can be viewed as having a formal LC of −2 (per formula unit), and therefore they should strongly attract interlayer K^+, causing a shortening of the K–O bonds. Alternatively, the electron depletion of the 2:1 layers can be viewed as causing basal O atoms to bind more tightly electron density donated by K to the K–O bonds. For model 2, where the affinity for an interlayer cation is formally zero (this model is similar to dispersing K metal atoms between charge neutral 2:1 layers as found in pyrophyllite), the open structure results. The basal oxygen atoms of the 2:1 layers can only interact weakly with electron density associated with interlayer K, resulting in longer K–O bonds and therefore an increase in the interlayer separation.

Because 2:1 layers in model 2 are made charge neutral by the addition of H atoms, it is natural to question whether interactions with H could be influencing the interlayer separation. The added H atoms complete the muscovite structural OH groups missing in model 1. The hydroxyls are situated at both the top and bottom of interlayer cavities and have unobstructed interaction with the interlayer cation. In dioctahedral micas, the H atom is well known to commonly deflect away from the octahedral sheet and into the siloxane cavities at an angle away from the basal plane normal, oriented toward the vacant octahedral site (Bailey, 1984). Our results are consistent with this behavior and suggest

Table 1. Optimized structural parameters for the various muscovite models in the primitive unit-cell, without symmetry. The cell parameters are given in Å and degrees and the atomic positions are fractional coordinates. In the Appendix, these data are transformed in terms of the conventional unit-cell with symmetry, but note that the atomic coordinates can be slightly modified during the transformation to fit the symmetry constraints exactly.

Model 1				Model 2				Models 3/4			
	a 5.1398	*b* 5.1393	*c* 20.2605		*a* 5.1771	*b* 5.1839	*c* 20.8538		*a* 5.1360	*b* 5.1462	*c* 20.8716
	α 92.567	β 92.594	γ 120.146		α 92.481	β 92.461	γ 120.268		α 92.606	β 92.765	γ 120.019
Al	0.1630	0.3260	0.0000	Al	0.1647	0.3294	−0.0004	Al	0.1807	0.3273	−0.0037
O1	0.5302	0.4139	0.0519	O1	0.5152	0.4117	0.0515	O1	0.5070	0.3805	0.0552
O2	0.1341	0.6225	0.0519	O2	0.1205	0.6254	0.0514	O2	0.1285	0.6348	0.0544
O3	0.9283	0.0161	0.0478	O3	0.9045	0.0175	0.0462	O3	0.8930	0.0155	0.0467
Si	0.5358	0.3882	0.1289	Si	0.5212	0.3899	0.1279	Si	0.5149	0.3775	0.1301
Si	0.1935	0.7038	0.1290	Si	0.1776	0.7033	0.1277	Si	0.1726	0.6960	0.1297
O4	0.3574	0.5378	0.1630	O4	0.3506	0.5481	0.1592	O4	0.3491	0.5419	0.1624
O5	0.4015	0.0548	0.1535	O5	0.3615	0.0542	0.1500	O5	0.3644	0.0460	0.1559
O6	0.8777	0.5785	0.1632	O6	0.8607	0.5708	0.1600	O6	0.8574	0.5602	0.1633
K	0.9013	0.0977	0.2498	K	0.9049	0.0954	0.2506	K	0.9024	0.0970	0.2500
Al	0.6738	0.8369	0.5000	Al	0.6712	0.8356	0.5002	Al	0.6728	0.8208	0.5034
O1	0.5864	0.4694	0.4482	O1	0.5861	0.4841	0.4484	O1	0.6149	0.4905	0.4447
O2	0.3774	0.8657	0.4480	O2	0.3757	0.8791	0.4485	O2	0.3661	0.8715	0.4455
O3	0.9824	0.0729	0.4525	O3	0.9837	0.0950	0.4536	O3	0.9833	0.1071	0.4531
Si	0.6128	0.4639	0.3712	Si	0.6106	0.4785	0.3721	Si	0.6223	0.4824	0.3699
Si	0.2969	0.8062	0.3710	Si	0.2960	0.8210	0.3723	Si	0.3039	0.8247	0.3702
O4	0.4626	0.6418	0.3371	O4	0.4521	0.6493	0.3407	O4	0.4581	0.6495	0.3376
O5	0.9460	0.5996	0.3465	O5	0.9452	0.6356	0.3490	O5	0.9533	0.6315	0.3438
O6	0.4235	0.1221	0.3368	O6	0.4332	0.1392	0.3404	O6	0.4424	0.1410	0.3370
Al	0.8372	0.6740	0.0000	Al	0.8358	0.6710	0.0000	Al	0.8465	0.6687	−0.0038
O1	0.4700	0.5861	−0.0519	O1	0.4853	0.5887	−0.0519	O1	0.4953	0.5866	−0.0458
O2	0.8661	0.3776	−0.0520	O2	0.8800	0.3751	−0.0518	O2	0.8936	0.3787	−0.0511
O3	0.0717	0.9839	−0.0479	O3	0.0957	0.9829	−0.0466	O3	0.1177	0.9808	−0.0462
Si	0.4644	0.6118	−0.1290	Si	0.4793	0.6105	−0.1283	Al	0.4735	0.6151	−0.1284
Si	0.8068	0.2962	−0.1290	Si	0.8227	0.2970	−0.1280	Si	0.8178	0.3013	−0.1303
O4	0.6429	0.4622	−0.1631	O4	0.6497	0.4522	−0.1597	O4	0.7229	0.5264	−0.1587
O5	0.5987	0.9452	−0.1535	O5	0.6393	0.9461	−0.1505	O5	0.5430	0.9660	−0.1439
O6	0.1225	0.4215	−0.1632	O6	0.1397	0.4298	−0.1605	O6	0.1169	0.3529	−0.1603
K	0.0985	0.9021	0.7502	K	0.0950	0.9044	0.7496	K	0.0954	0.9018	0.7500
Al	0.3260	0.1629	0.5000	Al	0.3283	0.1640	0.5002	Al	0.3322	0.1558	0.5039
O1	0.4135	0.5305	0.5519	O1	0.4135	0.5155	0.5520	O1	0.4131	0.5060	0.5457
O2	0.6224	0.1341	0.5520	O2	0.6238	0.1205	0.5519	O2	0.6220	0.1082	0.5511
O3	0.0174	0.9270	0.5475	O3	0.0159	0.9048	0.5469	O3	0.0195	0.8820	0.5460
Si	0.3870	0.5360	0.6289	Si	0.3889	0.5211	0.6283	Al	0.3862	0.5267	0.6283
Si	0.7029	0.1937	0.6290	Si	0.7037	0.1788	0.6281	Si	0.6996	0.1829	0.6303
O4	0.5371	0.3579	0.6630	O4	0.5473	0.3502	0.6598	O4	0.4740	0.2764	0.6587
O5	0.0538	0.4004	0.6536	O5	0.0544	0.3644	0.6515	O5	0.0356	0.4570	0.6446
O6	0.5765	0.8778	0.6632	O6	0.5664	0.8605	0.6600	O6	0.6481	0.8826	0.6595
				H	−0.2255	1.0245	0.0787	H	−0.2981	1.0119	0.0410
				H	−1.0282	0.2255	0.4214	H	−1.0132	0.2971	0.4602
				H	0.2265	−1.0238	−0.0790	H	0.2404	−1.0240	−0.0798
				H	1.0272	−0.2279	0.5786	H	1.0310	−0.2375	0.5798

Table 2. The optimized *c* axes and interlayer spacings for all the models, before and after Cs/K exchange (Å). The occupation of each of the two interlayer sites in the unit-cell is denoted as either K or Cs. The *c* axes for the primitive and conventional unit-cells are equivalent.

		c Axis		Interlayer spacing			
		Pre-exchanged	Cs exchanged	Pre-exchanged		Cs exchanged	
Model	LC			K	K	K	Cs
1	−2	20.261	20.641	3.64	3.64	3.63	4.06
2	0	20.854	20.920	3.88	3.88	3.92	3.94
3	−1	20.872	21.167	3.73	4.07[1]	3.72	4.40[1]
4	−1	20.872	21.062	4.07[1]	3.73	4.09[1]	3.97

[1] Al/Si substitution in both upper and lower tetrahedral sheets comprising this interlayer site (tetrahedral sheet composition = $AlSiO_5$).

https://doi.org/10.1346/CCMN.2001.0490603 Published online by Cambridge University Press

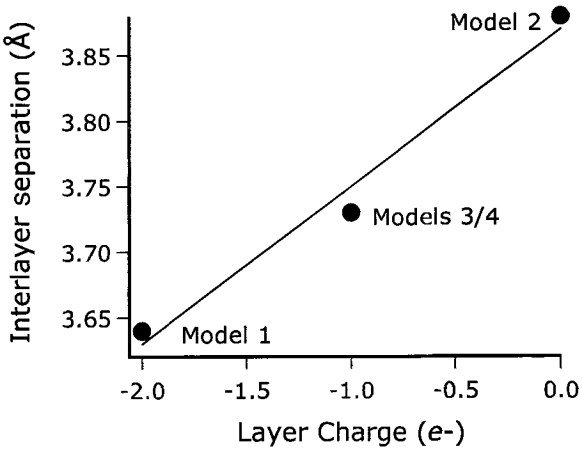

Figure 5. The change in the interlayer separation for the pre-exchanged muscovite models as a function of LC. For models 1 and 2, the separation at both interlayer sites within each is the same. For models 3 and 4, the separation differs because of the distortion of specific tetrahedral sheets in each model due to Al/Si substitutions. The separation graphed for models 3 and 4 are those for the undistorted site, to illustrate the regular dependence on LC.

that the degree of tilt away from the direction normal to the basal plane is ~43° for model 2 (K–H = 3.58 Å). This angle is significantly larger than estimations from neutron diffraction experiments (Rothbauer, 1971) and electrostatic energy calculations (Giese, 1984 and references therein), which range between 12 and 26°. Previous plane-wave GGA calculations indicate the angle is 22° in the dioctahedral layered silicate pyrophyllite. It is possible that calculated deflection angle is sensitive to the applied theory. We did not evaluate the energy as a function of deflection angle to test the validity of this result because of the required computational expense, leaving this matter as a subject for future work. For trioctahedral micas in which the OH group is forced to point directly into the interlayer site cavity, repulsion between hydroxyls and interlayer cations can play a significant role in the interlayer separation (Giese, 1975). However, for dioctahedral micas, K-H repulsion is accommodated by deflection of H in the direction of least resistance (*i.e.* towards the vacant octahedral site) and thus it is unlikely to affect the interlayer separation (Giese, 1984). Also, specifically in model 2, because of the slight electron excess and the low electronegativity of structural O^{2-}, the excess negative charge is likely to be shared between the cations, driving the effective charges on K and H closer to the neutral state and therefore decreasing the K–H interaction potential. Hence we assume that K–H interaction is not the primary cause of the difference in the interlayer separation between models 1 and 2.

The Al/Si substitutions in models 3 and 4 formally balance the formula unit of the muscovite structure. In both models, the LC is −1, falling between the extremes of models 1 and 2. Considering only LC for the moment, given the trends observed for models 1 and 2, an interlayer spacing that falls between 3.64 and 3.88 Å is expected. Because of structural distortions in the substituted tetrahedral sheets, this turns out to be true only for the undistorted interlayer sites (3.73 Å). Figure 5 shows the reasonably good correlation between the calculated interlayer spacing and the formal LC. The slope of the trend leads to a prediction of a −0.12 Å/*e*− dependence on LC.

Each Al/Si substitution results in longer tetrahedral site bonds which induces a misfit between the tetrahedral and octahedral sheets, leading to what are known as tetrahedral rotations (see Bailey, 1984). The strain is released by rotation of tetrahedra in the basal plane, which distorts the siloxane rings from hexagonal to ditrigonal. A measure of this distortion is given by the parameter $\alpha = \cos^{-1}(b_{sub}/b_{ideal})$, where the *b* parameters are the *b* axes (conventional unit-cell) for the substituted and non-substituted (ideal) cases. Using model 2 as the non-substituted ideal case, models 3 and 4 have $\alpha = 7.6°$, which falls within the typical range for dioctahedral micas of 6–19° (Bailey, 1984). The Al/Si substitutions drive a reduction in the lateral dimensions of the interlayer site which is counterbalanced with the drive to minimize the energy in the interlayer K–O bonds. The typical outcome is a propping open of the interlayer spacing. Our calculations are consistent with this behavior, as the distortion causes the interlayer spacing to increase by 0.34 Å to 4.07 Å.

It is also worthwhile to note the effect of Al/Si substitutions on OH orientations (Figure 6). Interestingly, the largest effect is not manifested on the most proximal OH group. Hydroxyls that normally point into a particular tetrahedral sheet are apparently unaffected when that Si_2O_5 sheet is converted to an $AlSiO_5$ sheet. By our definition earlier, the deflection angle remains close to 43°. However, OH groups belonging to the Si_2O_5 sheet on the opposite side of a 2:1 layer are deflected further away from their respective interlayer cation site, with the deflection angle ~90°. These results are suggestive of the high sensitivity of OH orientations to free electrical charges arising from tetrahedral substitutions, with a dependence on location. It seems likely that this opposing H atom is attracted to the charge localized at this particular tetrahedral site and is easily 'pulled' out of the siloxane cavities.

Cs-exchanged muscovite

For the Cs-exchanged models, some similarities to the pre-exchanged muscovite behavior are found in the trends for the Cs-substituted interlayer site. Cs^+ is a larger cation than K^+, having radii of 1.88 Å and 1.64 Å, respectively (Shannon, 1976), affording a qualitative explanation of differences in behavior to some degree. As for pre-exchanged models 1 and 2,

https://doi.org/10.1346/CCMN.2001.0490603 Published online by Cambridge University Press

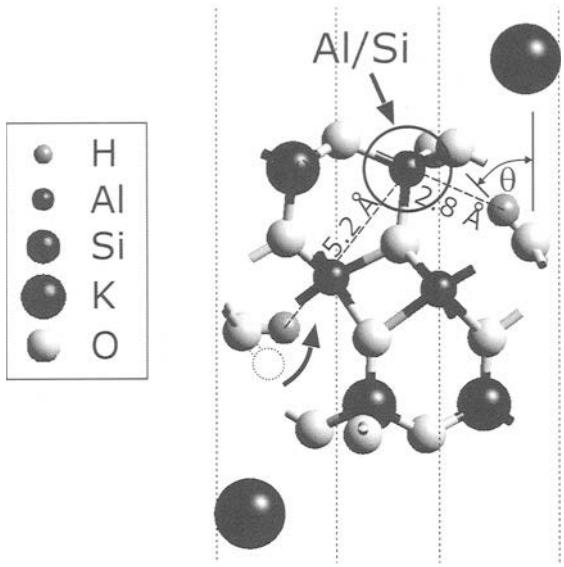

Figure 6. Ball and stick illustration detailing the change in OH orientation arising from tetrahedral Al/Si substitution. The deflection angle (θ) of the OH nearest the substituted site is unaffected, but the respective deflection angle of the more distant hydroxyl increases from ~43° to ~90°.

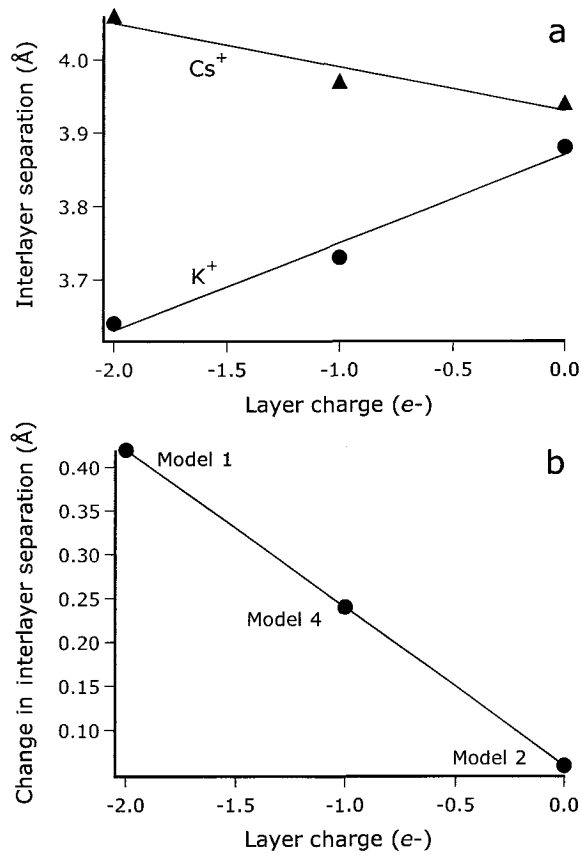

Figure 7. (a) A comparison of the dependence of the interlayer separation on LC for the pre-exchanged and Cs-exchanged muscovite models. (b) The difference of the data in (a), showing the interlayer modifications accompanying the Cs/K exchange. Model 3 is excluded because of the large effect of site distortion on the interlayer spacing at the exchange site, arising from Al/Si substitution.

Cs-exchanged model 2 has a larger c axis than for model 1 (Table 2). In passing, however, we note at this point that the difference, 0.28 Å, is much smaller. As for the pre-exchanged muscovite, most of this difference is accounted for by a change in the interlayer spacings. It turns out though that only the interlayer spacing occupied by K increases from model 1 to 2 (by 0.29 Å), whereas that occupied by Cs actually decreases slightly (by 0.12 Å). We explain the reversal of behavior in a later section.

The Al/Si substitution has effects similar to those found for the pre-exchange models. For Cs-exchanged model 3, where Al/Si-substituted tetrahedral sheets comprise the Cs interlayer site, the largest c axis dimension and Cs interlayer spacing results from tetrahedral rotations which distort the Cs site. The pattern of Al/Si substitutions is identical to that for the pre-exchange models, so presumably the driving force to distort the interlayer site is the same. But the coordination sphere of the larger Cs^+ cation can accommodate less distortion than that for K^+, causing a larger degree of propping open of the 2:1 layers. In model 3, Al/Si substitutions cause an increase in the Cs interlayer site to 4.40 Å, 0.68 Å larger than the undistorted K site and twice the increase demonstrated by the pre-exchanged model 3. As noted in a study of the structure of the Cs $2M_2$ mica nanpingite (Ni and Hughes, 1996), and implied in a study of the physical properties of biotites (Hewitt and Wones, 1975), the coordination sphere of the large Cs cation is more resistant to distortion than for smaller cations and hence tetrahedral rotations are hindered. Our calculations are consistent with this behavior. Using the Cs-exchanged model 2 as the ideal, undistorted structure, $\alpha = 2.6°$ for model 3 where Al/Si substitution is at the Cs site, and $\alpha = 7.1°$ for model 4 where Al/Si substitution is at the K site adjacent to the Cs site (which remained undistorted).

As for the pre-exchanged models 3 and 4, the Al/Si substitutions in the Cs-exchanged models 3 and 4 allow the interlayer spacings for the Cs interlayer to be examined for the formally balanced conditions where the LC = −1. The interlayer spacing at the Cs site was found to decrease with decreasing LC, in contrast to the behavior for interlayer K in both the pre-exchanged models, and the K site in the Cs-exchanged models (Figure 7a). Examining model 4, which captures the interlayer spacing for Cs unaffected by tetrahedral rotations, we find that the Cs interlayer spacing appropriately lies between models 1 and 2. The results demonstrate an interesting LC dependence for

https://doi.org/10.1346/CCMN.2001.0490603 Published online by Cambridge University Press

Table 3. Experimental thermodynamic (standard state = 298.15 K, 1 bar) used for the estimation of heats of hydration (ΔH_{HYD}), ionization potential (ΔH_{IP}) and entropy changes (ΔS) for the solvated cation component of the overall exchange reaction from (Wagman *et al.*, 1968, 1969).

ΔH^0_r (kJ/mol)			ΔH_{IP} (kJ/mol)	ΔH_{HYD} (kJ/mol)
$K^0_{(g)}$	$K^+_{(g)}$	$K^+_{(aq)}$	$K^0_{(g)} \rightarrow K^+_{(g)}$	$K^+_{(g)} \rightarrow K^+_{(aq)}$
89.24	514.26	−252.38	425.02	−766.64
$Cs^0_{(g)}$	$Cs^+_{(g)}$	$Cs^+_{(aq)}$	$Cs^0_{(g)} \rightarrow Cs^+_{(g)}$	$Cs^+_{(g)} \rightarrow Cs^+_{(aq)}$
76.06	457.96	−258.28	381.90	−716.24

S^0 (J/mol K)		$\Delta S_{T = 298.15\ K}$ (kJ/mol)
$K^0_{(g)}$	$K^+_{(aq)}$	$K^0_{(g)} \rightarrow K^+_{(aq)}$
160.34	102.5	−17.24
$Cs^0_{(g)}$	$Cs^+_{(aq)}$	$Cs^0_{(g)} \rightarrow Cs^+_{(aq)}$
175.60	133.05	−12.69
(kJ/mol)		$K^0_{(g)} + Cs^+_{(aq)} \rightarrow K^+_{(aq)} + Cs^0_{(g)}$
ΔH		−7.28
$T\Delta S$		−4.56
ΔG		−2.72

interlayer Cs of opposite sign and lesser magnitude (+0.06 Å/$e-$) than for interlayer K (−0.12 Å/$e-$). The trends converge to a similar interlayer spacing value for the condition LC = 0. Subtracting the data in Figure 7a gives the change in the interlayer separation as a function of LC (Figure 7b). The net dependence on LC is 0.18 Å/$e-$, indicating that the change in the interlayer spacing arising from Cs → K exchange will increase with more highly charged 2:1 layers.

The explanation for the observed behavior for K where the interlayer contracts as LC increases is intuitive. Increasing LC should attract interlayer cations more strongly and cause the 2:1 layers from either side to contract, binding the interlayer cations more tightly. That this trend should not be the case is indicative of a countering interaction, which we attribute to repulsion between the free electrical charges on the 2:1 layers. In the absence of interlayer cations, increasing the LC would have the effect of opening the interlayer spacing to relieve the build-up of Coulombic repulsion across the interlayer region. With interlayer cations present, these interactions are screened to some degree. Our calculations suggest indirectly that Cs^+ has a lower capacity to screen interlayer repulsions than K^+. This is probably based on a complicated combination of the relative effective nuclear charges (lower for Cs relative to K) and polarizabilities (higher for Cs relative to K) for these cations, and we chose not to scrutinize this independently in a quantitative way in this study. Some indication of the influence of cation size on the interlayer spacing, independent of 2:1 layer-layer repulsions, is seen in Figure 7a for the case where LC = 0. Nearly a complete loss of distinction in the interlayer spacing is apparent when there is no charge on the 2:1 layers. This indicates a lower sensitivity of the interlayer spacing to cation size and a higher sensitivity to LC. At the same time, with regard to the electronic characteristics of the interlayer cation, the calculations suggest that the net balance between the bonding attraction to the interlayer cation and 2:1 layer-layer repulsions reverses between that of K and Cs. A worthwhile test in future work would be to consider Rb as the interlayer cation.

Two final observations regarding the Cs-exchanged structures are noteworthy. The calculations demonstrate that the properties of the K site (the lower interlayer site in Figure 2) are independent of the adjacent Cs site, retaining the structural characteristics of the pre-exchanged K sites described above. This suggests that structural modifications due to interlayer cation exchange do not penetrate as far as interlayer sites in adjacent basal planes, provided that the structure is free to expand/contract. Also, no significant difference is found with respect to OH orientations and their behavior regarding tetrahedral substitutions in the Cs-exchanged models. The deflection angles are the same as described for the pre-exchange muscovite models (see Figure 6).

Exchange energetics

Using the total energies for the optimized structures combined with experimental data for the free interlayer cations, as described earlier (see Figure 4), the Cs → K exchange energy for constant pressure conditions can be estimated. Experimental thermodynamic data for the free cations are given in Table 3. As can be seen in the enthalpic terms, the smaller K^0 atom binds its valence electron more tightly and therefore has a higher ionization potential relative to Cs^0. But, at the same time, the small size of K^+ and higher effective nuclear charge interacts more strongly with water molecules in its hydration sphere and therefore its heat of hydration is lower than for Cs^+. A large fraction of the differences offset, leaving a relatively small negative enthalpic energy contribution from the cations to the forward exchange reaction (−7.3 kJ/mol). This small driving force is offset according to $\Delta G = \Delta H - T\Delta S$ by a net entropy decrease for the cations

https://doi.org/10.1346/CCMN.2001.0490603 Published online by Cambridge University Press

Table 4. Calculated constant pressure (1 bar) Cs/K exchange energetics for muscovite with and without the solvated free cation contribution. The energy data are in kJ/mol of primitive unit-cell (two formula units). Corresponding changes in the interlayer spacing at the exchange site and the change in the *c* axis dimension are given in Å. Note that the expansion of the *c* axis is due to only one of two possible Cs/K replacements in the unit-cell.

Exchange energy	Model 1	Model 2	Model 3	Model 4
$X(K) + Cs^0_{(g)} \rightarrow X(Cs) + K^0_{(g)}$	−2.6	13.1	18.1	3.0
$X(K) + Cs^+_{(aq)} \rightarrow X(Cs) + K^+_{(aq)}$	−5.3	10.4	15.4	0.3
Δ Int. spacing at ex. site	0.42	0.06	0.34	0.24
Δ *c* axis	0.38	0.07	0.29	0.19

of −4.6 kJ/mol at 298.15 K, leaving $\Delta G = -2.7$ kJ/mol with respect to the cation component of the overall exchange reaction in solution.

From the *ab initio* total energies, it turns out that the solid-phase components of the exchange energies are also quite small. Total energy differences with and without the free solvated cation contribution are given in Table 4. Also listed are the changes in the *c* axis dimension accompanying exchange. The constant pressure calculations allow for a net volume change (ΔV) and therefore it is possible to estimate the amount of energy that would be expended in reality to do work on the system by expansion to accommodate Cs in the interlayer. This work has the potential to affect the enthalpic part of the exchange energetics according to $\Delta H = \Delta E + P\Delta V$, where ΔE is the internal energy change, but the $P\Delta V$ work term with respect to the solid phase turns out to be ~3–4 orders of magnitude smaller than the overall exchange energetics. Furthermore, with respect to the solid phase, we assume the entropic contribution to be negligibly small because of the conservation of bond numbers at the interlayer site upon exchange. Therefore, the exchange energetics are largely a balance of the internal energy change in muscovite and free energies of the cations in solution.

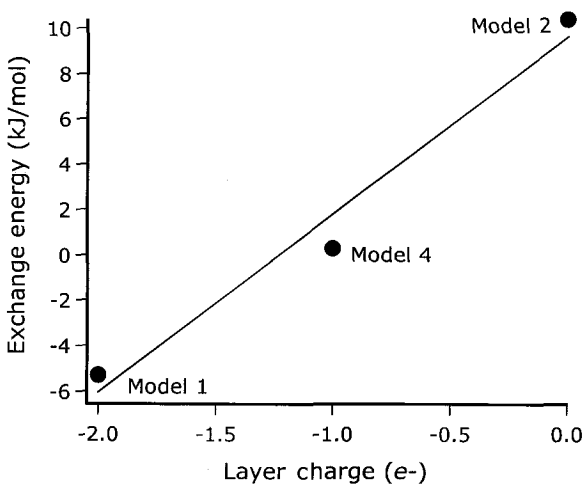

Figure 8. The relationship between the calculated Cs/K exchange energy and LC. The trend predicts that the forward exchange reaction becomes more strongly favored with increasing LC.

According to Table 4, the Cs/K exchange reaction is therefore very close to isoenergetic, with the energies for each of the models varying only by a few kJ/mol, at the same order of magnitude as the free solvated cation contribution. This result would undoubtedly not be the case for isovolumetric conditions where the forward exchange reaction would probably be large and unfavorable. The small exchange energy overall suggests that the muscovite structure is essentially indifferent with respect to interlayer cation when the interlayer spacing is free to change. Between the various models, the results indicate that the exchange energy systematically follows changes in this parameter, which in turn depends on LC. Setting aside model 3, which has a large effect of Al/Si substitutions on the exchange site, the remaining model exchange energies can be seen to be related to LC (Figure 8). Taking the simple hard-sphere perspective, that model 1 should be the most energetically favorable structure to incorporate a larger interlayer cation is somewhat counter-intuitive, given that it has the smallest initial interlayer spacing. The results are suggestive of the prevailing importance of the LC near the interlayer site relative to interlayer cation radius.

For the formally charge-balanced models, however, interlayer site distortions arising from Al/Si tetrahedral substitutions can be seen to have a strong deleterious effect on the forward driving force for exchange. For model 3, a decrease in α occurs from 7.6° to 2.6° after exchange, hinting at the strain injected into the tetrahedral sheets upon incorporation of Cs. A visual depiction of the distortion at the exchange site can be seen in electron density maps along a plane through one of the basal oxygen layers (Figure 9). The model 3 exchange is the least favored of all the models. Hence, interlayer cation size effects can be seen to be an important factor where the shape of the interlayer site is significantly distorted.

CONCLUSIONS

Ab initio calculations of a series of muscovite models reveal some important controls upon and structural modification due to the exchange of Cs for K in the interlayer site, including some insight into the energetics and the effects of LC and tetrahedral substitutions thereon. The built-in variation in stoichiometries under

https://doi.org/10.1346/CCMN.2001.0490603 Published online by Cambridge University Press

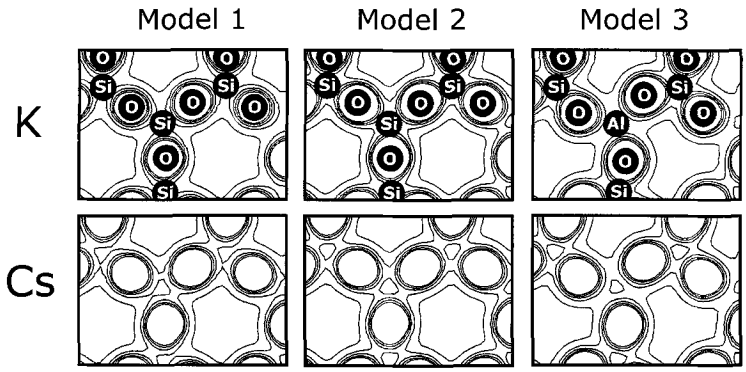

Figure 9. Electron density maps for a slice parallel to the basal plane approximately through the centers of basal O atoms. Site distortion arising from Al/Si substitution is clearly significant and reduces the size and changes the shape of the interlayer site.

a charge-neutral cell constraint is, to our knowledge, a novel mode of manifesting differing LC in the structure. In the absence of interlayer site distortion, relationships between LC and the interlayer spacing are clearly demonstrated, with a dependence on the interlayer cation. Presumably, the propensity to screen 2:1 layer-layer repulsions arising from LCs differs for K and Cs, to the point that an opposite response in the interlayer spacing occurs between them with a change in the LC. Interlayer K appears to screen 2:1 layer-layer repulsions better, whereby increasing the LC leads to smaller interlayer spacing, whereas the opposite response is found for interlayer Cs. Because isomorphic substitution disorder is typical in micas, LC is likely to be distributed heterogeneously across basal surfaces and laterally variable. Thus, even in interlayers uniformly occupied by one type of cation, a certain degree of strain in the interlayer region can be expected to be present following the lateral variation in charge, the degree of which should be smaller for interlayer Cs. The LC also appears to exert significant influence on the interlayer spacing and therefore the energetics of interlayer cation exchange for this system. Where site distortion is minimal, the forward exchange reaction becomes more favorable with increasing LC.

By comparison of the results of models 3 and 4, where LCs are equivalent and the formula unit balanced, some effects of Al/Si substitution on Cs $\rightarrow$ K exchange have been demonstrated. Consistent with known effects, tetrahedral rotations alter the bonding symmetry of the interlayer site, decreasing its size, causing the interlayer spacing to increase. In the absence of such distortions, this exchange system appears to be insensitive to interlayer cation size, as long as the unit-cell parameters are not constrained. Clearly, for a distorted site, the reduction in the size of the interlayer cavity heightens the sensitivity of the exchange energetics to cation size. Under these conditions, the exchange of the larger Cs cation for K is energetically unfavorable. Moreover, when the tetrahedral substitutions are not located at the exchange site, the structural modifications to the exchange site and the energetics for exchange were found to show systematic dependence on LC with structures where LC was distributed more homogeneously throughout. The behavior suggests that the effects of tetrahedral substitutions on the charge distribution in 2:1 layers are felt over distances significantly longer than T–O bond lengths.

Overall, the calculations suggest that the incorporation of Cs into muscovite interlayers is energetically feasible and nearly isoenergetic when the expansion of the interlayers is not inhibited. The results are consistent with Cs incorporation into frayed-edge sites. They are also consistent with slow Cs exchange rates into core interlayer regions of muscovite. We estimate the driving force for the overall exchange reaction to be very small and therefore the forward exchange behavior is likely to be dominated by diffusion kinetics. Likewise, any long-lived fixation of Cs in the interlayers of muscovite is probably due to kinetic barriers, rather than thermodynamics. At frayed-edge sites, where permanent LCs may be unsaturated with interlayer cations and larger interlayer spacings are available, the exchange process is known to be experimentally facile. Because of the predicted preference of Cs for larger interlayer sites in the presence of exposed LC, the calculations are indirectly consistent with this observation. Future calculations similar to these except under conditions of fixed, increased interlayer separations may be appropriate to confirm the nature of these relationships at frayed-edge sites.

ACKNOWLEDGEMENTS

During the course of this work, KMR and EJB were supported by Laboratory Directed Research and Development funds from Pacific Northwest National Laboratory. JRR was supported by the US Department of Energy, Office of Basic Energy Sciences, Engineering and Geosciences Division, contract 18328. Pacific Northwest Laboratory is operated for the US Department of Energy by Battelle Memorial Institute under Contract DE-AC06-76RL0 1830. We acknowledge the MSCF Computing Facility of the W.R. Wiley Environmental Molecular Sciences Laboratory for providing Computer resources for this work. We are also grateful to the National

Energy Research Supercomputing Center for a generous grant of computer time.

REFERENCES

Anderson, K. and Allard, B. (1983) Sorption of radionuclides on geologic media. *Report No. SKBF-KBS-TR-83-07.* Svensk Karnsbransterforjning.

Bailey, S.W. (1984) Crystal chemistry of the true micas. Pp. 13–57 in: *Micas* (S.W. Bailey, editor). Mineralogical Society of America, Washington, D.C.

Bradbury, M.H. and Baeyens, B. (2000) A generalised sorption model for the concentration dependent, uptake of caesium by argillaceous rocks. *Journal of Contaminant Hydrology,* **42,** 141–163.

Bridgeman, C.H. and Skipper, N.T. (1997) A Monte Carlo study of water at an uncharged clay surface. *Journal of Physics—Condensed Matter,* **9,** 4081–4087.

Bridgeman, C.H., Buckingham, A.D., Skipper, N.T. and Payne, M.C. (1996) Ab initio total energy study of uncharged 2:1 clays and their interaction with water. *Molecular Physics,* **89,** 879–888.

Brueeuwsma, A. and Lyklema, J. (1971) Interfacial electrochemistry of hematite (α-Fe_2O_3). *Discussions of the Faraday Society,* **52,** 324–333.

Burns, A.F. and White, J.L. (1963) Removal of potassium alters b-dimension of muscovite. *Science,* **139,** 39–40.

Cerius^2 User Guide (1997) *Cerius^2*. Molecular Simulations Inc.

Chang, F.R.C., Skipper, N.T. and Sposito, G. (1995) Computer simulation of interlayer molecular structure in sodium montmorillonite hydrates. *Langmuir,* **11,** 2734–2741.

Chatterjee, A., Iwasaki, T. and Ebina, T. (2000) A novel method to correlate layer charge and the catalytic activity of 2:1 dioctahedral smectite clays in terms of binding the interlayer cation surrounded by monohydrate. *Journal of Physical Chemistry A,* **104,** 8216–8223.

Comans, R.N.J., Haller, M. and Depreter, P. (1991) Sorption of cesium on illite—nonequilibrium behavior and reversibility. *Geochimica et Cosmochimica Acta,* **55,** 433–440.

Comans, R.N.J. and Hockley, D.E. (1992) Kinetics of cesium sorption on illite. *Geochimica et Cosmochimica Acta,* **56,** 1157–1164.

Cremers, A., Elsen, A., Depreter, P. and Maes, A. (1988) Quantitative analysis of radiocesium retention in soils. *Nature* **335,** 247–249.

De Carvalho, R. and Skipper, N.T. (2001) Atomistic computer simulation of the clay-fluid interface in colloidal laponite. *Journal of Chemical Physics,* **114,** 3727–3733.

De Preter, P., Vanloon, L., Maes, A. and Cremers, A. (1991) Solid liquid distribution of radiocesium in boom clay—a quantitative interpretation. *Radiochimica Acta,* **52-3,** 299–302.

Dolcater, D.L., Lotse, E.G., Syers, J.K. and Jackson, M.L. (1968) Cation exchange selectivity of some clay-sized minerals and soil materials. *Proceedings of the Soil Science Society of America,* **32,** 795–798.

Feller, D., Glendening, E.D., Woon, D.E. and Feyereisen, M.W. (1995) An extended basis set ab initio study of alkali metal cation water clusters. *Journal of Chemical Physics,* **103,** 3526–3542.

Garcia, A., Elsasser, C., Zhu, J., Louie, S.G. and Cohen, M.L. (1992) Use of gradient-corrected functionals in total energy calculations for solids. *Physical Review B,* **46,** 9829–9832.

Gibbs, G.V. (1982) Molecules as models for bonding in silicates. *American Mineralogist,* **67,** 421–450.

Giese, R.F., Jr. (1975) The effect of F/OH substitution on some layer-silicate minerals. *Zeitschift für Kristallographie,* **141,** 138–144.

Giese, R.F., Jr. (1984) Electrostatic energy models of micas. Pp. 105–144 in: *Micas* (S.W. Bailey, editor). Mineralogical Society of America, Washington, D.C.

Gillan, M.J. (1989) Calculation of the vacancy formation energy in aluminum. *Journal of Physics–Condensed Matter,* **1,** 689–711.

Greathouse, J. and Sposito, G. (1998) Monte Carlo and molecular dynamics studies of interlayer structure in $Li(H_2O)_3$-smectites. *Journal of Physical Chemistry B,* **102,** 2406–2414.

Gutierrez, M. and Fuentes, H.R. (1996) A mechanistic modeling of montmorillonite contamination by cesium sorption. *Applied Clay Science,* **11,** 11–24.

Hewitt, D.A. and Wones, D.R. (1975) Physical properties of some synthetic Fe-Mg-Al trioctahedral biotites. *American Mineralogist,* **60,** 854–862.

Hobbs, J.D., Cygan, R.T., Nagy, K.L., Schultz, P.A. and Sears, M.P. (1997) All-atom ab initio energy minimization of the kaolinite crystal structure. *American Mineralogist,* **82,** 657–662.

Jackson, M.L. (1963) Interlayering of expansible layer silicates in soils by chemical weathering. *Clays and Clay Minerals,* **11,** 29–46.

Kim, Y. and Kirkpatrick, R.J. (1997) Na-23 and Cs-133 NMR study of cation adsorption on mineral surfaces: local environments, dynamics, and effects of mixed cations. *Geochimica et Cosmochimica Acta,* **61,** 5199–5208.

Kim, Y., Kirkpatrick, R.J. and Cygan, R.T. (1996) Cs-133 NMR study of cesium on the surfaces of kaolinite and illite. *Geochimica et Cosmochimica Acta,* **60,** 4059–4074.

Kinniburgh, D.G. and Jackson, M.L. (1981) Cation adsorption by hydrous metal oxides and clay. Pp. 91–160 in: *Adsorption of Inorganics at Solid-Liquid Interfaces.* (M.A. Anderson and A.J. Rubin, editors). Ann Arbor Science, Michigan.

Kresse, G. and Furthmuller, J. (1996) Efficient iterative schemes for ab initio total-energy calculations using a plane-wave basis set. *Physical Review B—Condensed Matter,* **54,** 11169–11186.

Laird, D.A. (1996) Model for crystalline swelling of 2:1 phyllosilicates. *Clays and Clay Minerals,* **44,** 553–559.

Laird, D.A. (1999) Layer charge influences on the hydration of expandable 2:1 phyllosilicates. *Clays and Clay Minerals,* **47,** 630–636.

Maes, E., Vielvoye, L., Stone, W. and Delvaux, B. (1999) Fixation of radiocaesium traces in a weathering sequence mica $\rightarrow$ vermiculite $\rightarrow$ hydroxy interlayered vermiculite. *European Journal of Soil Science,* **50,** 107–115.

Mortland, M.M. (1958) Kinetics of potassium release from biotite. *Proceedings Soil Science Society of America,* **22,** 503–508.

Ni, Y.X. and Hughes, J.M. (1996) The crystal structure of nanpingite-$2M_2$, the Cs end-member of muscovite. *American Mineralogist,* **81,** 105–110.

Payne, M.C., Teter, M.P., Allan, D.C., Arias, T.A. and Joannopoulos, J.D. (1992) Iterative minimization techniques for ab initio total-energy calculations: molecular dynamics and conjugate gradients. *Reviews of Modern Physics,* **64,** 1045–1097.

Perdew, J.P. and Wang, Y. (1992) Accurate and Simple Analytic Representation of the Electron-Gas Correlation-Energy. *Physical Review B—Condensed Matter,* **45,** 13244–13249.

Rich, C.I. and Black, W.R. (1964) Potassium exchange as affected by cation size, pH, and mineral structure. *Soil Science,* **97,** 384–390.

Rothbauer, R. (1971) Untersuchung eines 2M1-muscovits mit Neutronenstrahlen. *Neues Jahrbüch für Mineralogie, Monatshefte,* **4,** 143–154.

Scott, A.D. and Reed, M.G. (1964) Expansion of potassium-depleted muscovite. *Proceedings of the 13th National Conference of the Clay Minerals Society, Clays and Clay Minerals,* **13,** 247–273.

Shannon, R.D. (1976) Revised effective ionic radii and systematic studies of interatomic distances in halides and chalcogenides. *Acta Crystallographica Section A: Crystal Physics, Diffraction Theoretical & General Crystallography,* **5,** 751–767.

Shroll, R.M. and Smith, D.E. (1999) Molecular dynamics simulations in the grand canonical ensemble: application to clay mineral swelling. *Journal of Chemical Physics,* **111,** 9025–9033.

Skipper, N.T., Refson, K. and McConnell, J.D.C. (1991) Computer simulation of interlayer water in 2:1 clays. *Journal of Chemical Physics,* **94,** 7434–7445.

Smith, D.E. (1998) Molecular computer simulations of the swelling properties and interlayer structure of cesium montmorillonite. *Langmuir,* **14,** 5959–5967.

Tamura, T., Bonner, W.P., Brinkley, F.S., Jacobs, D.G., Myers, O.H. and Murano, T. (1963) Mineral exchange studies. *Report—Oak Ridge National Laboratory, ORNL-3492,* pp. 62–70.

Vanderbilt, D. (1990) Soft self-consistent pseudopotentials in a generalized eigenvalue formalism. *Physical Review B,* **41,** 7892–7895.

Venkataramani, B., Venkateswarlu, K.S. and Shankar, J. (1978) Sorption properties of oxides. *Journal of Colloid and Interface Science,* **67,** 187–194.

Wagman, D.D., Evans, W.H., Parker, V.B., Halow, I., Bailey, S.M. and Schumm, R.H. (1968) Selected values of chemical thermodynamic properties. Tables for the first thirty-four elements in the standard order of arrangement. *United States National Bureau of Standards Technical Note,* **270-3,** 1–264.

Wagman, D.D., Evans, W.H., Parker, V.B., Halow, I., Bailey, S.M. and Schumm, R.H. (1969) Selected values of chemical thermodynamic properties. Tables for elements 35 through 53 in the standard order of arrangement. *United States National Bureau of Standards Technical Note,* **270-4,** 1–141.

Wang, J.W., Kalinichev, A.G., Kirkpatrick, R.J. and Hou, X.Q. (2001) Molecular modeling of the structure and energetics of hydrotalcite hydration. *Chemistry of Materials,* **13,** 145–150.

Weiss, C.A., Kirkpatrick, R.J. and Altaner, S.P. (1990) Variations in interlayer cation sites of clay minerals as studied by Cs-133 MAS nuclear magnetic resonance spectroscopy. *American Mineralogist,* **75,** 970–982.

White, J.A. and Bird, D.M. (1994) Implementation of gradient-corrected exchange-correlation potentials in Car-Parrinello total energy calculations. *Physical Review B—Condensed Matter,* **50,** 4954–4957.

White, J.L., Bailey, G.W., Brown, C.B. and Ahlrichs, J.L. (1962) Migration of lithium ions into empty octahedral sites in muscovite and montmorillonite. *Special Paper—Geological Society of America,* 295 pp.

Young, D.A. and Smith, D.E. (2000) Simulations of clay mineral swelling and hydration: dependence upon interlayer ion size and charge. *Journal of Physical Chemistry B,* **104,** 9163–9170.

E-mail: kevin.rosso@pnl.gov

(Received 6 October 2000; revised 2 April 2001; Ms. 491; A.E. Randall T. Cygan)

APPENDIX

Optimized structural parameters for the various muscovite models in terms of the conventional unit-cell with symmetry. The unit-cell parameters are given in Å and degrees and the atomic positions are in fractional coordinates. Models 1 and 2 converge to the space group *C*2/*c*, which is the $2M_1$ muscovite space group. In models 3 and 4, the chosen Al/Si tetrahedral substitutions break the symmetry to space group *C*2.

Model 1				Model				Models 3/4			
	a 5.1282	*b* 8.9086 β 95.178	*c* 20.2605		*a* 5.1595	*b* 8.9850 β 94.967	*c* 20.8538		*a* 5.1396	*b* 8.9055 β 95.379	*c* 20.8716
K	0.5000	0.4018	0.7500	K	0.5000	0.4051	0.7500	K	0.5000	−0.4022	0.0000
Al	0.2445	−0.0815	0.5000	Al	0.2459	−0.0820	0.5004	Al	0.7465	0.0748	0.2536
Si	0.4615	0.0745	0.6289	Si	0.4548	0.0664	0.6285	Si	0.5518	−0.0694	0.1200
Si	0.4482	−0.2546	0.6290	Si	0.4409	−0.2621	0.6283	Si	0.5642	0.2610	0.1206
O1	0.4719	0.0585	0.5519	O1	0.4643	0.0513	0.5522	O1	0.5522	−0.0616	0.1948
O2	0.3782	−0.2441	0.5520	O2	0.3718	−0.2514	0.5521	O2	0.6186	0.2534	0.1958
O3	0.4721	0.4548	0.5476	O3	0.4604	0.4448	0.5471	O3	0.5443	−0.4375	0.2030
O4	0.4475	−0.0896	0.6630	O4	0.4485	−0.0982	0.6600	O4	0.5535	0.0963	0.0878
O5	0.2271	0.1733	0.6536	O5	0.2093	0.1551	0.6517	O5	0.7918	−0.1601	0.0938
O6	0.7271	0.1507	0.6633	O6	0.7134	0.1476	0.6602	O6	0.2911	−0.1504	0.0870
				H	0.3990	−0.6273	0.5788	H	0.3957	−0.6338	0.3296
								K	0.5000	0.4038	0.5000
								Al	0.2435	−0.0879	0.2540
								Al	0.4561	0.0707	0.3785
								Si	0.4406	−0.2579	0.3803
								O1	0.4592	0.0470	0.2959
								O2	0.3644	−0.2565	0.3011
								O3	0.4508	0.4317	0.2964
								O4	0.3747	−0.0984	0.4088
								O5	0.2461	0.2110	0.3949
								O6	0.7651	0.1180	0.4098
								H	−0.3578	0.6547	0.2108